Journal of Molecular Graphics and Modelling 98 (2020) 107610

Contents lists available at ScienceDirect

Journal of Molecular Graphics and Modelling

journal homepage: www.elsevier.com/locate/JMGM

Construction of atomic models of full hepatitis B vaccine particles at different stages of maturation

Laurent Berthier [a, 1], Olivier Brass [b, 1], Gilbert Deleage [a], Raphaël Terreux [a, *]

[a] PRABI-LG – Laboratoire de Biologie Tissulaire et d'ingénierie Thérapeutique (LBTI), UMR, UCBL, CNRS 5305, Université de Lyon, 7 Passage du Vercors, 69367, Lyon Cedex 07, France
[b] Sanofi Pasteur, avenue Ch. Mérieux, F-69280, Marcy-l'Etoile, France

ARTICLE INFO

Article history:
Received 20 December 2019
Received in revised form
2 March 2020
Accepted 27 March 2020
Available online 9 April 2020

Keywords:
ab-initio modeling
Docking
HBsAg particle
HBV
Iterative threading
MDFF
Molecular dynamics
Molecular modeling

ABSTRACT

Hepatitis B, one of the world's most common liver infections, is caused by the Hepatitis B Virus (HBV). Via the infected cells, this virus generates non pathogen particles with similar surface structures as those found in the full virus. These particles are used in a recombinant form (HBsAg) to produce efficient vaccines. The atomic structure of the HBsAg particles is currently unsolved, and the only existing structural data for the full particle were obtained by electronic microscopy with a maximum resolution of 12 Å. As many vaccines, HBsAg is a complex bio-system. This complexity results from numerous sources of heterogeneity, and traditional bio-immuno-chemistry analytic tools are often limited in their ability to fully describe the molecular surface or the particle. For the Hepatitis B vaccine particle (HBsAg), no atomic data are available so far. In this study, we used the principal well-known elements of HBsAg structure to reconstitute and model the full HBsAg particle assembly at a molecular level (protein assembly, particle formation and maturation). Full HBsAg particle atomic models were built based on an exhaustive experimental data review, amino acid sequence analysis, iterative threading modeling, and molecular dynamic approaches.

1. Introduction

Hepatitis B virus (HBV – *Hepadnaviridiae family)* causes Hepatitis B and consequent liver diseases. Prevention against HBV has progressed over the past 30 years through vaccination [1]. Nevertheless, HBV remains a constant threat in the field of public health; (890 million deaths worldwide in 2015) [2] and improvement of a vaccine for an extensive use is a perpetual challenge. Virus-like particle (HBsAg) based HBV vaccine is the most used antigenic form, and it is composed of only one protein (HBs) and phospholipids (PLs). The HBsAg structure and antigenicity have been largely described by a panel of molecular, structural and immuno-biochemistry approaches and results [3–50].

Besides, HBs protein can adopt different surface arrangements in the Hepatitis B/D viruses, HBsAg particles, or in microtubes [22–28]. All these conformations are generated in long, multistep bioprocesses, in and out of cells or yeast [29]. In every case, a maturation step of the particle has been described after their yeast extraction or cell secretion, which lasted between a minimum of 60–120 h [11] to a maximum of 23 days [19], depending on the parameters used in the process. At 37 °C and in presence of potassium isothiocyanate (KSCN) [11,12], the 10–20% particle size increase observed during HBsAg maturation [25,26] was faster and reflects a spontaneous molecular reorganization as a function of the intra- and extra-cellular environments.

The HBsAg particle phospholipid content (HBs/di-oleoyl-phosphatidylcholine [DOPC] ratio is about 60/40%) [3–8], and their detailed interactions with their environment has been described [9–13]. Published experimental data are largely dependent upon the time of observation of the HBsAg synthesis/maturation. These published results have to be discussed in the context of our model, which enabled us to reconstitute the chronological and molecular assembly of the HBsAg particle. In this matter, published results on different HBsAg particles (from"a-d/y-w/r" subtypes [14–16]), with mammalian or yeast origins [17,18] produced by different bioprocesses and controlled by different bio-analyzes [19,50], were compared for similarities and overlaps. These overlaps were used to reconstitute and model the chronological and molecular dynamics

* Corresponding author.
E-mail address: raphael.terreux@ibcp.fr (R. Terreux).
[1] authors have an equal contribution to this work.

https://doi.org/10.1016/j.jmgm.2020.107610
1093-3263/

of the HBsAg particle during its assembly. The integration of these experimental similarities observed between all the HBsAg particles at different stages of formation and maturation involves: particle size [20–24], size variation during maturation [25,26], particle density [20], composition and protein/PL ratio [3,4,6], surface/volume of the spikes [22–25], and the number of asymmetric units per particle, which remains controversial.

Many structural data are available to this day: electron microscopy (EM) profile models [23,24], atomic force microscopy (AFM) [22] and X-ray scattering data [27], in which the spikes are considered as HBs oligomer-condensed subunits in interaction with surrounding PLs. Mammalian [24] or yeast [23] HBsAg particles, cryo-EM, and 3D image reconstructions at 12 Å showed the same PL-protein scaffold with a density of 24 spikes per particle with a similar and remarkable spike and surface morphology. Large and small size subpopulations (20.6 ± 0.8 nm; 22.5 ± 0.6 nm) of the same mass were observed with an octahedral symmetry. The potential molecular evolution from small to large particles was modeled through a conformational switch between two molecular asymmetric units [24]. This could explain the size increase and spike profiling during the maturation [22–25].

The necessary plasticity/flexibility of the molecular antigenic surface during the particle maturation has been described as mainly resulting from the cross-bridging of the 14 strongly conserved cysteines of the HBs sequence [30] and their switching networks of S–S bonds during the HBs particle genesis [31,32]. Among the 14 cysteines found in each HBs monomer, 10 are considered being key amino acids during the particle formation [29,31,35–48] through an intra/inter S–S dynamic switch evolution [38–42]. In spite of this, the network of disulfide bond is not yet clearly established (e.g. the same cysteine residues have been shown to be part of inter/intramolecular S–S bonds or as free SH groups [29,38–42] which may be dependent upon the time of observation). Furthermore, HBs synthesis and its progressive oligomeric organization are dependent upon a specific membrane phospholipid environment in which the organization of PLs is not well described. In spite of this, the efficient levels of immune protection provided by HBs particle vaccines obtained from different yeast strains and different processes suggest that the final epitopic surface conformations have similarities [17]. These epitopes are recognized by specific monoclonal antibodies (mAbs) and depend on the level of the particle maturation and antigenicity. Thus, mAbs provide a useful tool to determine which kind of S–S network can fit the experimental results. This is especially useful for discontinuous epitopes [49], for which different segments of the HBs sequence need to be located in a surface smaller than 1000 $Å^2$ (the size of the epitope-paratope interactive surface). This method can also help to clarify the molecular transformations occurring during the particle maturation and was used to challenge our models of the HBsAg particles.

2. Results

In this study, we managed to compile all the available data to propose an atomic model of the HBsAg particle, in order to better understand its organization and conformation. This work can help to improve the HBV vaccine design and formulation. Experimental results and associated surface molecular structures described in the literature were combined to develop a multi-threading HBs protein model, which was used to reconstitute two HBsAg particle models. Molecular dynamics of the whole particle models were performed to better understand 1) the difference in size of the two models of the particle. 2) the distinct domains, orientation and oligomerization of HBs monomers 3) the organization of HBs proteins with PLs.

The HBsAg particle is composed of a finite number of the HBs protein. The HBs sequence is 226 residues long. Considering the published HBs particle electronic microscopy density profiles for the small and large particles [24], we can observe that both particles present a “snub cube” configuration, which agrees with an octahedral symmetry. A snub cube is composed of 60 edges, 6 squares and 32 equilateral triangles. As modeled [23], HBs proteins characterized by electronic profiles occupy 24 equilateral triangles, which form 12 pairs of triangles joined along one edge. These pairs of triangles with two antigenic spikes are the elementary asymmetric units, composed of 4, 6 or 8 copies of the proteins (there is some controversy in the litterature [23,24]), leading to a total number of 48, 72 or 96 copies of the protein per particle. The last surfaces of 6 squares and 8 equilateral triangles, which are not observable by electronic microscopy, are filled by PLs.

Controversy about the HBs protein number is due to the lack of HBs atomic model. To this day, there is no experimental structure of the HBs protein due to the current impossibility of its crystallization. Homology modeling is not reliable, because no relevant template can be found in the PDB (maximum similarity is about 10%). However, a secondary structure prediction through the Antheprot [51] software was conducted. The residue composition reveals a low number of charged residues (especially negatively charged residues). Several secondary structure prediction methods were tested, resulting in the prediction of a hydrophobic α-helix structure for 3 segments (T5-N40, H60–I100, I150–I226), with a leucine zipper from L77 to L98.

Alternatively, a 3D model was generated using the Iterative Threading ASSEmbly Refinement (I-TASSER) method [52]. A network of intramolecular S–S bonds was used as constraints (C107–C138, C137–C149 and C139–C147)[38–40]. Four protein models were generated and ranked by model Confidence (C-score) [53] and structural class identity protein quality (TM-Score). The optimal C-score was obtained at 4.1 (with high confidence), with a

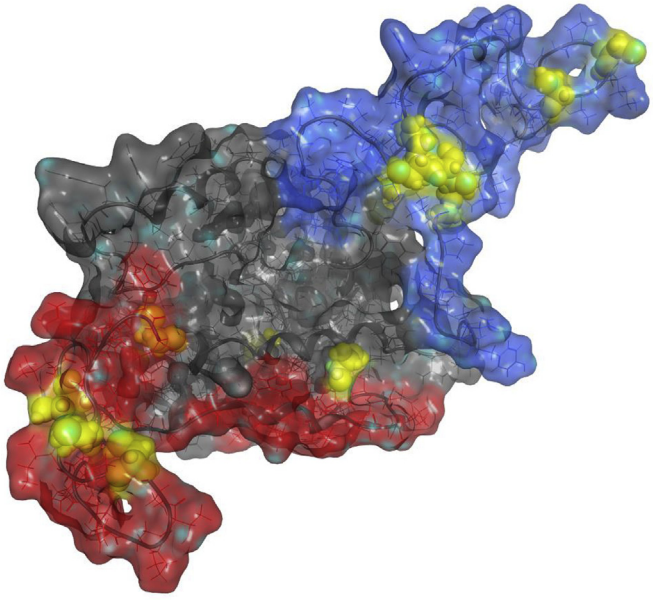

Fig. 1. Model of the monomeric HBs protein obtained after I-TASSER modelling. The model is displayed as a ribbon superimposed with all the protein atoms. The secondary structures are in agreement with the consensus secondary structure predictions method integrated in Antheprot [51]. The AGL sequence (D99-F180), which is very flexible, is exposed to the solvent and colored in blue. The α-helix core, which forms the rigid central domain, is shown in grey. The HCL (R23-C90), which is internalized in the particle, is colored in red. The cysteines of each domain are represented by yellow spheres. Disulfide bonds (C107–C138, C137–C149 and C139–C147) are used as constraints in the I-TASSER software and were created using the MOE software.

TM-score of 0.28 and an optimal average accuracy for the HBs model shown in Fig. 1 of approximately 4 Å. The selected model agreed with the secondary structure predictions. This HBs monomer model was energetically optimized and submitted to protein-protein docking [54] in order to construct a dimer model.

Despite the lack of identity between their sequences, it has been shown that non-related viral proteins sharing similar function can exhibit a significant structural resemblance [55]. In order to investigate any common structural feature between our HBs model and any other known capsidial viral protein, we used the CATH [56] server to perform a broad structural verification which did not lead to any significant result.

The selected dimer model agreed with the exposure to solvent with a low energy of −630 kJ/mol (high stability). In this model, the AGL sequence (99–160) and the HCL or interacting capsid sequence (23–90) are oriented towards opposite sides, which may result in inner (for the HCL) and outer (for the AGL) orientations in the complete particle. Using epitope mapping [49], several antibodies were able to recognize other non-AGL sequences such as 158–175, 186–207, and 208–226, which suggests an external orientation. The other dimer models had residues identified in the epitope mapping, which were internalized, or presented large hydrophobic surfaces exposed to the solvent, and were thus discarded. The selected HBsAg dimer model was prepared and minimized with the Molecular Operating Environment (MOE) software. The resulting model is displayed in Fig. 2. Using the same protocol and the dimer model, tetramers were constructed. In the selected tetrameric model, the four HBs proteins have their HCL cysteines located in the same spatial region, which allows for the creation of intermolecular S–S bridges, as experimentally observed [38]. This complex was extended to a multimeric form by addition of new dimers to the tetramer. Models of tetramers, hexamers and octamers were built using this approach. For each model, an 8° angle of rotation between the dimers was able to induce a curvature on the inner face of the particle. As for the dimer analysis, other models were not suitable with this kind of arrangement. The best dimer, tetramer, hexamer and octamer models were adjusted to the electronic profiles (Chimera software [57], but only the tetrameric form had a good fit with the experimental data and yielded the best correlation score (0.63 for Electron Microscopy Data: EMD-1158 and 0.66 for EMD-1159) without overlapping structures, in an almost parallel orientation relative to the surface of the particle. Next, molecular dynamics were performed on the tetramer model and coefficients of correlation increased from 0.63 to 0.85 for the EMD-1158, and from 0.66 to 0.93 for the EMD-1159. The quality of the electronic profile adjustment confirmed that the observed molecular "beams" are composed of tetramers built as a dimer of dimers. The resulting model is shown in Fig. 2.

Based on this tetrameric model, the protein skeleton/scaffolds were designed to obtain the two atomic models of the full HBsAg particles. The EMD profiles of the large and small particles observed by Gilbert et al. [24] were used as guidelines to integrate the tetramer repetitive structures (i.e. the beams) in the octahedral, snub-cube symmetric particle. For both small and large particles, 12 repetitive and symmetrical beam models were docked and fitted to the EMD profiles. Phospholipids organized in DOPC bilayer membranes were added to the particle structure to fill the remaining empty surfaces with low or no electronic density. For this matter, a square and planar model measuring 100 × 100 Å of DOPC bilayer membrane was generated with the membrane builder of the VMD molecular viewer. Then, the membrane model was fitted in the vacant space according to the hydrophobic surfaces of the surrounding proteins. Finally, all the DOPC molecules being too close (less than 1 Å) of a HBs protein were removed. This process was performed for the 6 squares and the 8 equilateral triangles of the large particle model, and only for the 6 squares of the small particle, which does not possess equilateral triangles. The quantity of added PLs was adjusted to the known ratio of content (HBs/DOPC ratio being about 60/40%) [3–8], for both models.

The small and large models were inserted in a TIP3P/[Na^+, Cl^-] 0.15 M solvent box. For each model, a molecular dynamic simulation was performed during 100 ns in order to relax the system. For both simulations, S–S bonds were reduced [5,20] and converted into free SH groups, in order to check the atomic stability of the particle. As shown in Fig. 3, both HBsAg particle models agree with the experimental EM data in term of spatial organization, with an EMD recovery of 85 and 93%, respectively for the small and large particles.

Both particles were stable during all the MD simulation and remained spherical. DOPC molecules undergo an optimization of their positions and make contacts with the adjacent HBs proteins. The analysis of the different energy terms of the forcefield reveals that the dynamics reach their equilibrium after 2 ns. After the simulations, the measured size of the particles was 198 ± 16 Å and 225 ± 10 Å, respectively for the small and the large particle. As first described by Gilbert et al. [24], and then by Mulder et al. [23] and indirectly by Short et al. [28] (22 nm in diameter for the HBs microtubes), the experimental structures of the small and large particles (respectively 18–20 nm and 22 nm) correspond to the two sub-populations previously observed before and after maturation [22–25]. Therefore, we propose that the immature particles correspond to the small sub-population, whereas the immunologically mature particles correspond to the large sub-population. During the yeast particle maturation, spikes are observed on the

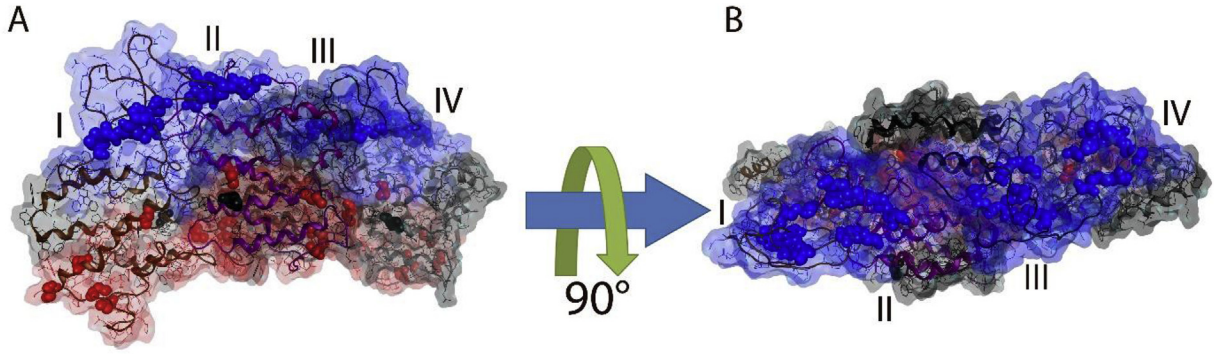

Fig. 2. Tetrameric HBs beam (2 dimeric asymmetric units). The model of the tetramer (a dimer of dimers) is displayed with monomers I, II, (first dimer) and III, IV (second dimer). Surfaces are colored in blue for the AGL loop (99–178) and in red for the capsid loop (23–90). The rest of the sequence is colored in grey. Figure B is the view from the outside of the particle view and figure A is rotated 90° along the y axis.

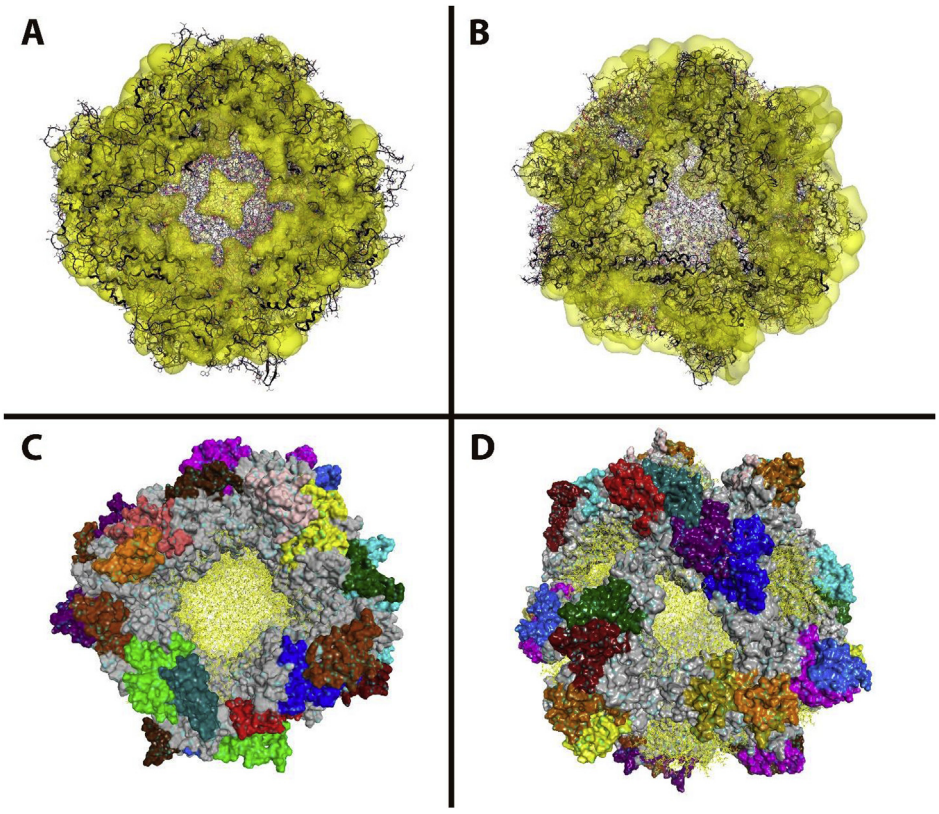

Fig. 3. Atomic models of the small (left: A/C) and large (right: B/D) particle. Upper panel (A/B): For each particle (small and large), all the atoms are superimposed with the cryo-EM density (small EMD-1158/large EMD-1159) with a transparent yellow iso-surface. The small and large model are displayed with black ribbons and lines for protein and grey line only for DOPC phospholipid. Both models are in good agreement with the EM densities. Because of its flexibility, the AGL loop sometimes overflows the iso-surface. This may explain why it is not well resolved on the surface of the particle. Lower panel (C/D): The solvent surface for proteins was computed and colored in grey, except for the 48 AGL loops (99–178) which were colored by chain. DOPC molecules were displayed as yellow lines.

particle surface, which agrees with our models. The spikes obtained in the large particle have a height of 2.5 ± 0.5 nm above the surface of the proteolipid cortex (4.0 ± 0.2 nm of thickness), with a half-height diameter of 3.9 ± 0.2 nm, and an inter-spike distance of 7.9 ± 0.4 nm.

The transformation between the two states could be explained by a change in the internal network of the disulfide bonds, as illustrated in Fig. 4. This shift could be described as a molecular diaphragm motion, as illustrated in Fig. 4A/4B and in Supplementary Video S1. This sliding shift mechanism may explain the whole reorganization of the particle. It should be noted that in the immature configuration, only triangular patches of PLs are observed, whereas both triangular and square PL patches are found in the mature particles.

Supplementary video related to this article can be found at https://doi.org/10.1016/j.jmgm.2020.107610

A visualization of the discontinuous epitope on the surface of the model is shown in Fig. 5 (partial tetrameric surface view). This figure is based on an experimental epitope mapping performed with various monoclonal antibodies recognizing continuous and discontinuous epitopes [49]. The three epitopes corresponding to the mAb H5 (Fig. 5A), H35 (Fig. 5B), and H53 (Fig. 5C) of the HBsAg surface were analyzed in order to check the final proximity of the discontinuous sequences. Discontinuous sequences recognized by the mAbs are 101–106 and 158–167 for H5, 121–130 and 166–175 for H35 and finally 186–207 and 112–117 for H53. All the recognized surfaces are less than 1000 $Å^2$, which is a suitable size for an antigenic recognition site. In every case, both sequences are contiguous and accessible for intermolecular interactions, which suggests that the different sequences of the discontinuous epitopes are correctly positioned on the surface of the particle. The proximity of the surfaces and their accessibility were not set as constraints in the model during the particle construction process.

3. Discussion

During this study, our main concern was to validate our models at the two different maturation times of the HBsAg particle, which structure at an atomic resolution remains unsolved. Our goal was to take into account various direct and indirect biological information to build models and validate them.

3.1. Two types of particles and diameter of the particles

The particle assembly follows these different steps: HBs synthesis, dimerization; and then formation of the oligomeric HBs scaffold, before the antigenic maturation in the extracellular compartment. The reconstitution of this chronological sequence helped to explain the discrepancies in the published data, which were linked to different times of observation. The particle antigenic maturation is a slow process (20 days at 23 °C), which involves surface reorganization and infrequent biochemical events. At 37 °C and in presence of an oxidant, the maturation time was reduced to 90 h. The final antigenicity obtained with these particles appeared to be sufficient for vaccinal use [11]. The structuration of the particle during its maturation relies on the dynamics of the intra/inter S–S networks, combined with other factors such as the formation of leucine zippers, lipid-protein junctions, and particle-solvent interactions.

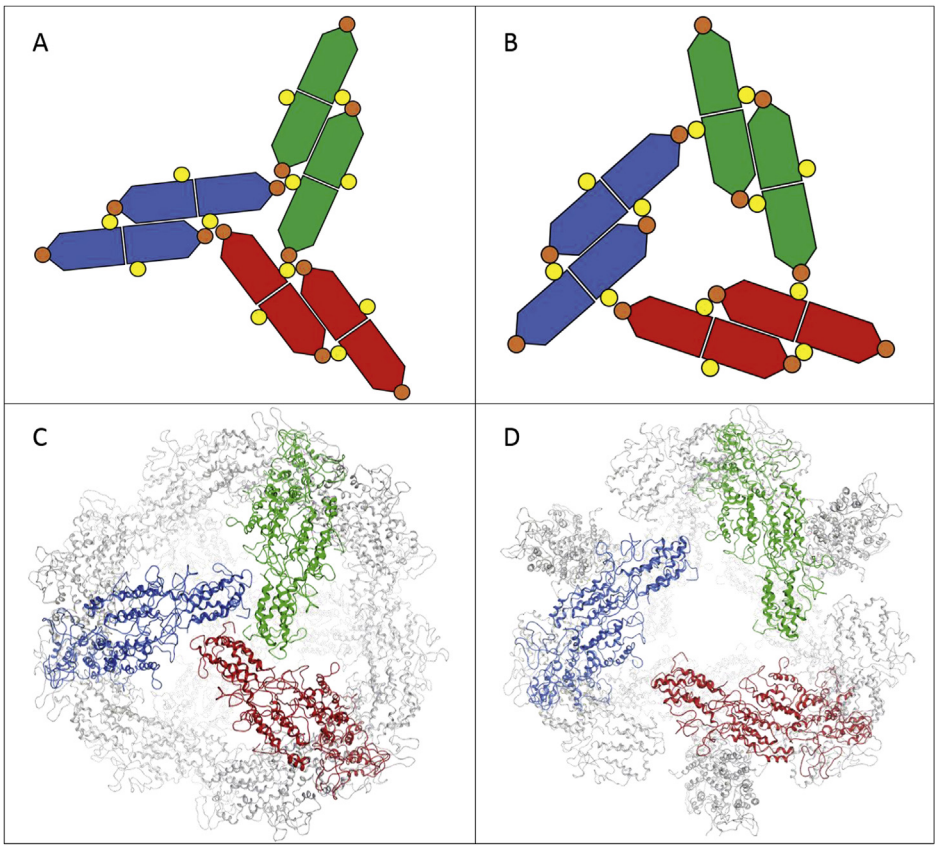

Fig. 4. Open/closed molecular diaphragm model. Panel A/C: "small" or closed conformation particle. Panel B/D "large" or open configuration particle. For each particle, the lower picture (C/D) displays the three tetramers with ribbon representation. The upper figures (A/C) are schematic views of the tetramers. Each tetramer is formed by the association of two adjacent dimers. Small orange balls represent a cluster composed of C65, C69, C48 and C76. Yellow balls represent C221. In the immature conformation, the tetramers are bound to each other by S—S bonds established between C76 (in orange) of the first tetramer and C221(in yellow) of the second tetramer. Conversely, in the mature particle, these disulfide bridges are established between C76 (in orange) of the first tetramer and C221 (in yellow) of the other dimer of the second tetramer. The switch to the open conformation is produced by rotation/translation, breaking the disulfide bonds to create new ones between orange (C76) and yellow (C221) balls.

The particle assembly coming from an initial protein-lipid scaffold assembly, followed by a slow maturation from the immature to the antigenic particle. Antibody studies have shown that the maturation process includes a structural modification of the exposed AGL sequence [11,12] through molecular mechanisms that are not yet fully understood. In yeast HBsAg particle, the immature particles obtained after yeast disruption are characterized by a single small size population [25]. Particles of the adw2 serotype produced by *Hansenula polymorpha* have an average diameter of approximately 18 nm before maturation, and 22 nm (unpublished data) or 23 nm[22] afterwards. A larger than 10% size increase was observed during the maturation process with another subtype (ayw), in which the particle diameters were found to be 17 and 22 nm[20]. Compared to the *in situ* HBV infection, in which particles are continuously secreted from infected cells, two co-existing particle subpopulations have been detected in blood samples with 18—20 and 22 nm sizes [24]. Similarly, differences in size between HBs particles of yeast and mammalian origin support the assumption that in both expression systems, 18—20 nm corresponds to the immature particles and 22—23 nm to the mature state.

3.2. Validation of the global organization of the particles

The results of the molecular dynamic simulations (100 ns) for the two particle models overlapped by more than 90% with the EM electronic profiles of the small and large particles [24], with respect to their octahedral symmetry, PL/HBs protein ratio and spikes organization. Spikes clearly appear in the large particles for previously observed forms [23]. Experimental spike detection was difficult at a resolution of 12 Å[24], probably because the flexible loops of the AGL sequences is less rigid than the core of the particle, especially during the unfolded immature stage. Whereas the surface protein scaffold is well characterized as a rigid and stable pseudo-capsid structure [23,24], the exact organization of the proteins on the particle surface still remains hypothetical, with the number of HBs monomers per particle varying between 48 and 100[22—28]. Different HBs model conformations (mono, di, tri, tetramer of HBs by asymmetric unit) were studied, and various factors such as the exposed side of the HCL/AGL sequences, the orientation of the polar surface and α-helix apolar core, and the steric hindrance of the HBs monomer were taken into account. The fit between the two final models and the experimental EM electronic profiles was scored by integration e.g., of the specific HBs volume, its dimer-unit organization, the PL/protein ratio, and the particle geometry/surface dimensions. In comparison with non-favored HBs organizations resulting from 1) a non-realistic atomic density (with more than 48 HBs/particle), 2) a non-realistic surface cortex thickness (except at near parallel HBs orientation relative to the surface of the particle), 3) the HCL and AGL not being correctly exposed (inside/outside of the particle, respectively), and finally, 4) HBs sequence analyses being more directed to a scaffold organization than a trans-membrane organization, only the dimer model being parallel to the surface fitted well with the EM electronic

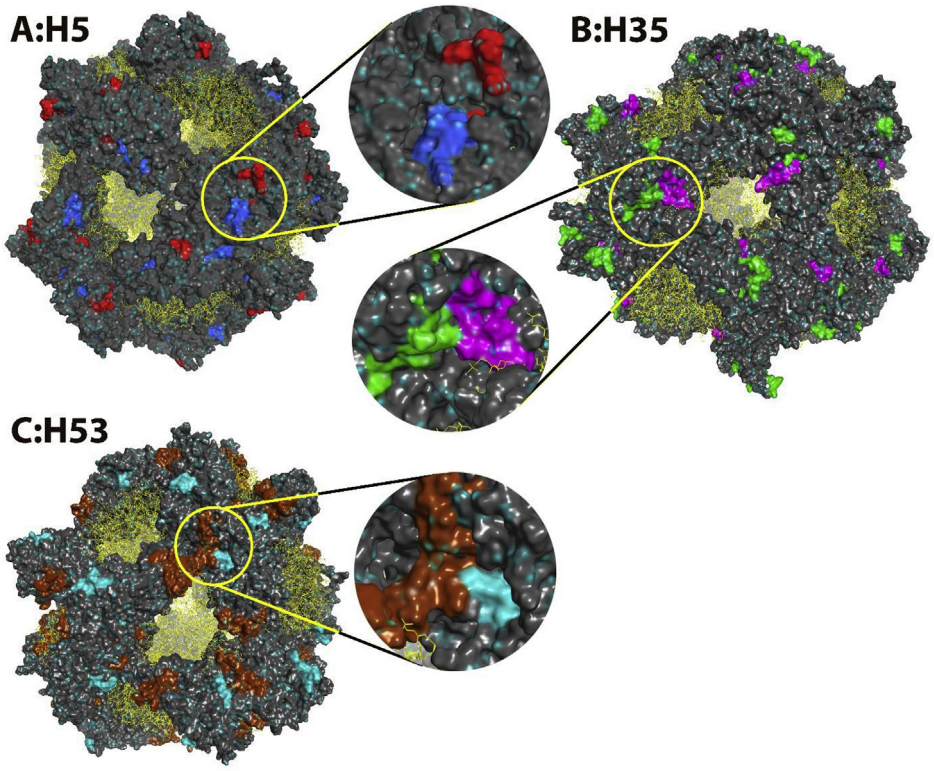

Fig. 5. Discontinuous epitope localization. Surface representation of the open particle model. The protein surfaces are displayed in grey, except for the sequences involved in the epitopes, which are displayed with colors. Phospholipids are displayed in yellow lines. The three epitopes corresponding to the mAb H5 (Fig 5A), H35 (Fig 5B), and H53 (Fig 5C) of the HBsAg surface are displayed in colors in order to check the final proximity of the discontinuous sequences. All the colored surfaces are less than 1000 $Å^2$, which is a suitable size for an antigenic recognition site. These surfaces, corresponding to the Ab binding sites and epitope sequences, are identified by three circles, and magnified aside. Discontinuous sequences recognized by Abs are for: H5 (red: 101–106/blue:158–167); H35 (green: 121–130/pink: 166–175) and H53 (light blue: 186–207, maroon: 112–117).

profiles. HBs dimer positioning at the surface of the particle agrees with the dimensions which were experimentally determined using different methods before and after maturation with the corresponding evolution of the spikes. Thickness of the particle cortex, height, diameter and volume of the spikes in both our models were quite similar to the published data.

3.3. Spike protrusions

The size of the spike protrusions was measured at 2.2 ± 0.8 nm (mid-height diameter of 3.9 ± 0.4 nm) with an inter-spike distance ranging from 5 to 6.5 nm[22]. Similar diameters of 4 nm were observed (3 nm spike height, 4 nm cortex thickness) for adr HBsAg particles synthesized in *Saccharomyces cerevisae* [18] and for the adw strain in the same yeast production system (2.2 nm spike height [23], 4.4 nm cortex thickness, 7–9 nm inter-spike distance). Using mammalian-derived particles, similar dimensions were obtained using a combination of electronic microscopy [24] and X-ray scattering [27] for particle or microtube [28] HBs structure, with a spike-based diameter of 7.5 nm, a height of 3 nm, a distance between spikes of 10 nm and a surface cortex of 4 or 5.6 nm for a particle with a diameter of 18.3–19.6 nm (adw particle from chronic Human carrier).

Other characteristics, such as surface and spike heterogeneity were analyzed in order to understand the potential transformations between the immature and the immunogenic stage. Spikes (AGL sequences) were apparent in both the mature and the immature state with a progressive evolution of morphology during the maturation [25]. Surface morphology was similar when comparing "yeast HBsAg" and "mammalian HBs particles" [22–24]. An accelerated change in the surface morphology was observed following redox and heat treatment [12,25]. During the maturation, the modifications of the S–S network and its associated AGL cysteine bridges are reversibly and temporarily reduced, before changing to a more rigid spike structure. After disruption of yeast cells, or secretion from mammalian cells, the HBsAg environment of the particle changes from an intra-cellular membrane system dedicated to HBs synthesis and oligomerization (first stable immature particle [5,20]) to an aqueous extracellular media in which particles mature. In both environments, the molecular mechanisms will be distinct, and the spontaneous maturation is probably driven by a reduction in the free enthalpy of the particle system in the new environment. Before maturation, non-covalent particle structures [5,20] and fully covalently S–S bound particles [38] were described. A study of the HBsAg maturation time indicated a progressive increase in the number of the S–S bonds [5], which was accelerated by redox treatment, pH elevation, heat and light [5,25]. This suggests that the 8 cysteines present at the surface of the flexible AGL sequence are reduced before maturation, refolded as a function of the decrease of the free enthalpy (environment changes), and inter and intramolecular S–S networks are reshuffling after redox reducer dialysis. The number of free thiol groups detected in yeast or mammalian HBsAg particles is time dependent when the maturation process is analyzed. It has been shown that 1 to 3 free thiols can be observed before maturation, but none were detectable afterwards [38–41]. This indicates that the S–S network involves all of the 8 AGL HBs cysteines. At the exception of the isolated C107, the seven other cysteines are clustered in 3 areas, which may increase their reactive thiol proximity: a triple contiguous cysteine sequence (137-138-139), a small loop

C121-X-X-C124 and a C147-X-C149 short cysteine sequence. The proximity and density of cysteines (being all located in an area smaller than 2500 Å^2), combined with the AGL sequence flexibility may favor the cysteine rearrangement in new stabilized S–S networks. Due to these changes in the S–S intra- and inter-molecular networks, the AGL epitope surfaces may adopt a different conformation leading to an improvement of their antigenicity during the maturation process.

3.4. Phospholipids and antigenicity

The role of PLs is essential for the particle formation, maturation and antigenicity. Their replacement has been assessed experimentally, and the particle antigenicity was improved using selected PLs [7]. Nevertheless, the structure and role of PLs is not yet clearly understood. Using NMR data [48], water has been shown to be present on both sides of the envelope of the particle. The limited diffusion of lipids [8] is not typical of bilayer membrane, although the packing of PLs in independent patches between the HBs protrusions [22,24] may explain this limited diffusion. The impermeability of the particles has been demonstrated [6] and indicates that the envelope structure is a "tight proteo-lipidic junction network". As HBsAg particles contain fewer lipids than typical enveloped viruses, a discontinuous bilayer membrane with strong interactions between the hydrophobic α-helix core and the PLs seems to be realistic. This specific discontinuous PL bilayer membrane occupies the empty surfaces (no electronic density by electronic microscopy) in the pseudo-capsidial HBs protein scaffold and generates a hermetic and rigid particle with entrapped solvent molecules, PLs, and triglycerides [48]. As these internal lipids are in an aqueous environment, they may be organized in liposomes, micelles, and nanoparticles or they could be bound to the internal PL surface of the particles. During the transformation from immature to mature or small to large particles, the diameter and the volume of the particles will increase without any change in their molecular weight. Thus, these lipids might act as a PL reservoir that participates in the maturation of the HBsAg particles.

3.5. Assumption of the mechanism of transition between small and large particles

In order to better understand the maturation of the spikes, an overlap of the electronic profiles [24] of the small and large particles was performed using our models. Surprisingly, the transition between the closed (small) and open (large) conformations makes the spikes harder to distinguish using cryo-EM profiles with a 12 Å resolution. Observations from the atomic model and EM data [23,24] suggest that the changes in the molecular structure during maturation correspond to an open and closed molecular system, which could be described as a “molecular diaphragm” in which the three blades of the diaphragm would be formed by three tetramers. During the opening of the molecular diaphragm, the tips of the three tetramers would mutually slip along the adjacent tetramers. In the open mature configuration, the repositioning of the cysteines would result in new intra- and intermolecular S–S bridges for a final more rigid and stable S–S network.

This molecular process is expected to generate a new antigenic surface detectable by specific mAbs directed against folded AGL sequences [12]. The correct overlap and folding of the experimental epitope of the HBs surface with the atomic surface organization of the model is a prerequisite for model validation. This will be especially true with discontinuous epitopes for which the different sequences of the HBs implicated in the Ab recognition should be in a near proximity (surfaces smaller than 1000 Å^2 which roughly corresponds to a paratope/epitope interaction surface). This validation was initiated using published experimental epitope mapping [49] and the initial results were satisfying regarding discontinuous epitope configuration and localization. Our antigenic surface description was confirmed by the first discontinuous epitope-Ab overlaps (H5, H35, H53). Ongoing and planned investigations will challenge these findings using different potential AGL S–S networks coupled with additional insights in the HBsAg particle antigenicity.

4. Conclusion

This study presents the first atomic model of a whole Hepatitis B vaccine particle created using modeling and molecular dynamics. Our model can be used as a basis to explain heterogeneous and conflicting observations previously published. Our two models are in good agreement with the published cryo-EM electronic profiles or the AFM surface characterization [22–24]. An atomic recovery of 90% at a 12 Å resolution [24] was obtained with our overlapping atomic models for the small and large size subpopulations of HBsAg particles. Through these models, the number of HBs monomers per particle (48), their orientation, organization, oligomerization and interactions with PLs and the surrounding molecules were validated. The size variation between the immature and mature HBsAg particles was also observed at the Sanofi Pasteur facility during the HBV vaccine particle maturation process and was correlated with an increase in antigenicity and antibody cross-reactivity for HBsAg particles of yeast and mammalian origins (in-house data from Sanofi Pasteur). The opening mechanism of the particle through the rearrangement of the SS bridge network was investigated, but more biological studies are needed for this to be conclusive. This model provides a better understanding of the molecular changes occurring during the particle maturation and can be used to optimize formulation for the HBsAg particle vaccine in the future.

5. Material and methods

Modelling. An *ab-initio* model was built using the HBs sequence [53] (UniprotKB P03141-3) and the I-TASSER software (Iterative Threading ASSEmbly Refinement) [54]. Two S–S bond networks were set and used as constraints to build 4 models of the protein. All the models were checked, and the best model was selected according to the C-score function [55]. This model was energetically optimized using the MOE2016 software with the AMBER10:EHT force-field [56] using protein default parameters.

Molecular Docking and Fitting. The optimized model was used with the ClusPro protein-protein docking algorithm to construct a dimer model. The ClusPro server [51] was used for all the protein-protein docking simulations. The protein-protein docking simulations were set up without proximity constraints. The simulation created several models. In order to validate the best model, we used accessibility data for the AGL and HCL sequences by checking their inner or outer localization on the particle, as residues 23–90 (HCL) interact with the capsid (inner side), and residues 99–178 (AGL) form the antigenic loops (outer side) in the full functional virus. The ClusPro balanced score was selected as the most relevant score in this case.

Several models of the dimer of dimer were then created by protein-protein docking using the ClusPro docking server. The model with the best ClusPro balanced score also had the best fit with the cryo-EM density data. This model was then duplicated and fitted into the complete cryo-EM density with the help of the Fit option of the UCSF Chimera Map module [52]. The tetramer assembly was then refined by flexible fitting to the cryo-EM density using the Molecular Dynamics Flexible Fitting (MDFF) method [52]. This protocol was applied to the 1158 and 1159 cryo-EM density.

Simulation Details. MDFF simulations were performed using the NAnoscale Molecular Dynamics (NAMD) 2.12 software. The CHARMM36 force field was used for all the calculations. The protein scaffold of the particles was simulated in vacuum and the dielectric constant was set to 80. Temperature was set at 300 K using Langevin dynamics with a damping constant of 5 ps^{-1}. The grid scaling (a MDFF parameter, which controls the balance between the map-derived potential energy term and the normal MD force field) was set to 0.3. Harmonic restraints were applied to preserve the correct chirality, the peptide bond configuration, and the secondary structure elements. MDFF simulations were performed until the convergence of the protein RMSD (Root-Mean-Square Deviation) was reached.

The 1,2-Dioleoyl-sn-glycero-3-phosphocholine (DOPC) molecules were then added to the system and solvated in a TIP3P water box with a 12 Å padding in every direction. Na^+ and Cl^- ions were added with a concentration of 0.15 M in order to neutralize system. A preequilibrated bilayer of DOPC lipids was added accordingly to the PPM web-server [58] placement recommendation. A total of 782 DOPC lipids for the closed form and 827 for the open form were added. A 100 ns trajectory was generated using the AMBER16 package with the ff14SB [59] and lipid14 [60] force fields in the NPT (Number Pressure and Temperature) ensemble in order to relax the system. For long-range electrostatic terms, the Particle-Mesh Ewald (PME) algorithm was used with non-bonded and van der Waals cut-offs of 10 Å. The temperature of the simulations was set to 300 K using Langevin thermostat, a pressure of 1 bar was used with an integration time step of 2 fs, and periodic boundary conditions were applied.

Acknowledgement

The authors would like to thank Jean Haensler and Régis Gervier from Sanofi Pasteur, as well as Simon Megy and Emmanuel Bettler from IBCP for their participation to this work.

Appendix A. Supplementary data

Supplementary data to this article can be found online at https://doi.org/10.1016/j.jmgm.2020.107610.

Funding

This work was supported by the Sanofi Pasteur company.

References

[1] GBD 2015 Disease and Injury Incidence and Prevalence Collaborators, Global, regional, and national incidence, prevalence, and years lived with disability for 310 diseases and injuries, 1990-2015: a systematic analysis for the global burden of disease study 2015, Lancet Lond. Engl. 388 (10053) (2016) 1545–1602, https://doi.org/10.1016/S0140-6736(16)31678-6.
[2] WHO, Hepatitis B Fact Sheet, 2018, 2018.
[3] F. Gavilanes, J.M. Gonzalez-Ros, D.L. Peterson, Structure of hepatitis B surface antigen. Characterization of the lipid components and their association with the viral proteins, J. Biol. Chem. 257 (13) (1982) 7770–7777.
[4] F. Gavilanes, J. Gomez-Gutierrez, M. Aracil, J.M. Gonzalez-Ros, J.A. Ferragut, E. Guerrero, D.L. Peterson, Hepatitis B surface antigen. Role of lipids in maintaining the structural and antigenic properties of protein components, Biochem. J. 265 (3) (1990) 857–864.
[5] D.E. Wampler, E.D. Lehman, J. Boger, W.J. McAleer, E.M. Scolnick, Multiple chemical forms of hepatitis B surface antigen produced in yeast, Proc. Natl. Acad. Sci. U.S.A. 82 (20) (1985) 6830–6834.
[6] V.J. Greiner, C. Egelé, S. Oncul, F. Ronzon, C. Manin, A. Klymchenko, Y. Mély, Characterization of the lipid and protein organization in HBsAg viral particles by steady-state and time-resolved fluorescence spectroscopy, Biochimie 92 (8) (2010) 994–1002, https://doi.org/10.1016/j.biochi.2010.04.014.
[7] J. Gómez-Gutiérrez, I. Rodríguez-Crespo, D.L. Peterson, F. Gavilanes, Reconstitution of hepatitis B surface antigen proteins into phospholipid vesicles, Biochim. Biophys. Acta 1192 (1) (1994) 45–52, https://doi.org/10.1016/0005-2736(94)90141-4.
[8] O. Satoh, M. Umeda, H. Imai, H. Tunoo, K. Inoue, Lipid composition of hepatitis B virus surface antigen particles and the particle-producing human hepatoma cell lines, J. Lipid Res. 31 (7) (1990) 1293–1300.
[9] J. Jezek, D. Chen, L. Watson, J. Crawford, S. Perkins, A. Tyagi, L. Jones-Braun, A heat-stable hepatitis B vaccine formulation, Hum. Vaccine 5 (8) (2009) 529–535, https://doi.org/10.4161/hv.5.8.8600.
[10] L.J. Braun, J. Jezek, S. Peterson, A. Tyagi, S. Perkins, D. Sylvester, M. Guy, M. Lal, S. Priddy, H. Plzak, et al., Characterization of a thermostable hepatitis B vaccine formulation, Vaccine 27 (34) (2009) 4609–4614, https://doi.org/10.1016/j.vaccine.2009.05.069.
[11] Q. Zhao, V. Towne, M. Brown, Y. Wang, D. Abraham, C.B. Oswald, J.A. Gimenez, M.W. Washabaugh, R. Kennedy, R.D. Sitrin, In-depth process understanding of RECOMBIVAX HB® maturation and potential epitope improvements with redox treatment: multifaceted biochemical and immunochemical characterization, Vaccine 29 (45) (2011) 7936–7941, https://doi.org/10.1016/j.vaccine.2011.08.070.
[12] Q. Zhao, Y. Wang, D. Abraham, V. Towne, R. Kennedy, R.D. Sitrin, Real time monitoring of antigenicity development of HBsAg virus-like particles (VLPs) during heat- and redox-treatment, Biochem. Biophys. Res. Commun. 408 (3) (2011) 447–453, https://doi.org/10.1016/j.bbrc.2011.04.048.
[13] B. Böttcher, N. Tsuji, H. Takahashi, M.R. Dyson, S. Zhao, R.A. Crowther, K. Murray, Peptides that block hepatitis B virus assembly: analysis by cryomicroscopy, mutagenesis and transfection, EMBO J. 17 (23) (1998) 6839–6845, https://doi.org/10.1093/emboj/17.23.6839.
[14] E. Guerrero, P.D. Swenson, P.S. Hu, D.L. Peterson, The antigenic structure of HBsAg: study of the d/y subtype determinant by chemical modification and site directed mutagenesis, Mol. Immunol. 27 (5) (1990) 435–441, https://doi.org/10.1016/0161-5890(90)90168-y.
[15] E. Ben-Porath, J.R. Wands, R.A. Marciniak, M.A. Wong, L. Hornstein, R. Ryder, M. Canlas, A. Lingao, K.J. Isselbacher, Structural analysis of hepatitis B surface antigen by monoclonal antibodies, J. Clin. Invest. 76 (4) (1985) 1338–1347, https://doi.org/10.1172/JCI112108.
[16] P. Valenzuela, P. Gray, M. Quiroga, J. Zaldivar, H.M. Goodman, W.J. Rutter, Nucleotide sequence of the gene coding for the major protein of hepatitis B virus surface antigen, Nature 280 (5725) (1979) 815–819, https://doi.org/10.1038/280815a0.
[17] D. Diminsky, R. Schirmbeck, J. Reimann, Y. Barenholz, Comparison between hepatitis B surface antigen (HBsAg) particles derived from mammalian cells (CHO) and yeast cells (Hansenula polymorpha): composition, structure and immunogenicity, Vaccine 15 (6–7) (1997) 637–647, https://doi.org/10.1016/s0264-410x(96)00239-3.
[18] M. Yamaguchi, K. Sugahara, K. Shiosaki, H. Mizokami, K. Takeo, Fine structure of hepatitis B virus surface antigen produced by recombinant yeast: comparison with HBsAg of human origin, FEMS Microbiol. Lett. 165 (2) (1998) 363–367, https://doi.org/10.1111/j.1574-6968.1998.tb13171.x.
[19] W.J. McAller, E.H. Wasmuth, Hepatitis B Surface Antigen Vaccine Production, 1976. US4088748A.
[20] P. Valenzuela, A. Medina, W.J. Rutter, G. Ammerer, B.D. Hall, Synthesis and assembly of hepatitis B virus surface antigen particles in yeast, Nature 298 (5872) (1982) 347–350, https://doi.org/10.1038/298347a0.
[21] K.H. Heermann, U. Goldmann, W. Schwartz, T. Seyffarth, H. Baumgarten, W.H. Gerlich, Large surface proteins of hepatitis B virus containing the pre-s sequence, J. Virol. 52 (2) (1984) 396–402.
[22] P.-E. Milhiet, P. Dosset, C. Godefroy, C. Le Grimellec, J.-M. Guigner, E. Larquet, F. Ronzon, C. Manin, Nanoscale topography of hepatitis B antigen particles by atomic force microscopy, Biochimie 93 (2) (2011) 254–259, https://doi.org/10.1016/j.biochi.2010.09.018.
[23] A.M. Mulder, B. Carragher, V. Towne, Y. Meng, Y. Wang, L. Dieter, C.S. Potter, M.W. Washabaugh, R.D. Sitrin, Q. Zhao, Toolbox for non-intrusive structural and functional analysis of recombinant VLP based vaccines: a case study with hepatitis B vaccine, PloS One 7 (4) (2012), e33235, https://doi.org/10.1371/journal.pone.0033235.
[24] R.J.C. Gilbert, L. Beales, D. Blond, M.N. Simon, B.Y. Lin, F.V. Chisari, D.I. Stuart, D.J. Rowlands, Hepatitis B small surface antigen particles are octahedral, Proc. Natl. Acad. Sci. U.S.A. 102 (41) (2005) 14783–14788, https://doi.org/10.1073/pnas.0505062102.
[25] Q. Zhao, Y. Wang, D. Freed, T.-M. Fu, J.A. Gimenez, R.D. Sitrin, M.W. Washabaugh, Maturation of recombinant hepatitis B virus surface antigen particles, Hum. Vaccine 2 (4) (2006) 174–180, https://doi.org/10.4161/hv.2.4.3015.
[26] V.J. Greiner, C. Manin, E. Larquet, N. Ikhelef, F. Gréco, S. Naville, P.-E. Milhiet, F. Ronzon, A. Klymchenko, Y. Mély, Characterization of the structural modifications accompanying the loss of HBsAg particle immunogenicity, Vaccine 32 (9) (2014) 1049–1054, https://doi.org/10.1016/j.vaccine.2014.01.012.
[27] L.P. Aggerbeck, D.L. Peterson, Electron microscopic and solution X-ray scattering observations on the structure of hepatitis B surface antigen, Virology 141 (1) (1985) 155–161, https://doi.org/10.1016/0042-6822(85)90192-8.
[28] J.M. Short, S. Chen, A.M. Roseman, P.J.G. Butler, R.A. Crowther, Structure of hepatitis B surface antigen from subviral tubes determined by electron cryomicroscopy, J. Mol. Biol. 390 (1) (2009) 135–141, https://doi.org/10.1016/j.jmb.2009.04.059.
[29] A.P. Huovila, A.M. Eder, S.D. Fuller, Hepatitis B surface antigen assembles in a post-ER, pre-golgi compartment, J. Cell Biol. 118 (6) (1992) 1305–1320, https://doi.org/10.1083/jcb.118.6.1305.

[30] H. Norder, B. Hammas, S. Löfdahl, A.M. Couroucé, L.O. Magnius, Comparison of the amino acid sequences of nine different serotypes of hepatitis B surface antigen and genomic classification of the corresponding hepatitis B virus strains, J. Gen. Virol. 73 (Pt 5) (1992) 1201–1208, https://doi.org/10.1099/0022-1317-73-5-1201.
[31] J. Salisse, C. Sureau, A function essential to viral entry underlies the hepatitis B virus "a" determinant, J. Virol. 83 (18) (2009) 9321–9328, https://doi.org/10.1128/JVI.00678-09.
[32] D. Tleugabulova, Size-exclusion chromatographic study of the reduction of recombinant hepatitis B surface antigen, J. Chromatogr. B Biomed. Sci. Appl. 713 (2) (1998) 401–407, https://doi.org/10.1016/s0378-4347(98)00181-9.
[33] C. Kreutz, Molecular, immunological and clinical properties of mutated hepatitis B viruses, J. Cell Mol. Med. 6 (1) (2002) 113–143, https://doi.org/10.1111/j.1582-4934.2002.tb00317.x.
[34] R. Prange, R. Nagel, R.E. Streeck, Deletions in the hepatitis B virus small envelope protein: effect on assembly and secretion of surface antigen particles, J. Virol. 66 (10) (1992) 5832–5841.
[35] B.E. Eble, V.R. Lingappa, D. Ganem, The N-terminal (pre-S2) domain of a hepatitis B virus surface glycoprotein is translocated across membranes by downstream signal sequences, J. Virol. 64 (3) (1990) 1414–1419.
[36] B.E. Eble, V.R. Lingappa, D. Ganem, Hepatitis B surface antigen: an unusual secreted protein initially synthesized as a transmembrane polypeptide, Mol. Cell Biol. 6 (5) (1986) 1454–1463, https://doi.org/10.1128/mcb.6.5.1454.
[37] B.E. Eble, D.R. MacRae, V.R. Lingappa, D. Ganem, Multiple topogenic sequences determine the transmembrane orientation of the hepatitis B surface antigen, Mol. Cell Biol. 7 (10) (1987) 3591–3601, https://doi.org/10.1128/mcb.7.10.3591.
[38] C.M. Mangold, F. Unckell, M. Werr, R.E. Streeck, Analysis of intermolecular disulfide bonds and free sulfhydryl groups in hepatitis B surface antigen particles, Arch. Virol. 142 (11) (1997) 2257–2267, https://doi.org/10.1007/s007050050240.
[39] C.M. Mangold, F. Unckell, M. Werr, R.E. Streeck, Secretion and antigenicity of hepatitis B virus small envelope proteins lacking cysteines in the major antigenic region, Virology 211 (2) (1995) 535–543, https://doi.org/10.1006/viro.1995.1435.
[40] C.M. Mangold, R.E. Streeck, Mutational analysis of the cysteine residues in the hepatitis B virus small envelope protein, J. Virol. 67 (8) (1993) 4588–4597.
[41] E. Guerrero, D.L. Peterson, F.G.G. Franco, Model for the Protein Arrangement in HBsAg Particles Based on Physical and Chemical Studies, 1988.
[42] H.J. Stirk, J.M. Thornton, C.R. Howard, A topological model for hepatitis B surface antigen, Intervirology 33 (3) (1992) 148–158, https://doi.org/10.1159/000150244.
[43] R. Prange, C.M. Mangold, R. Hilfrich, R.E. Streeck, Mutational analysis of HBsAg assembly, Intervirology 38 (1–2) (1995) 16–23, https://doi.org/10.1159/000150410.
[44] R. Prange, R.E. Streeck, Novel transmembrane topology of the hepatitis B virus envelope proteins, EMBO J. 14 (2) (1995) 247–256.
[45] G. Wounderlich, V. Bruss, Characterization of early hepatitis B virus surface protein oligomers, Arch. Virol. 141 (7) (1996) 1191–1205, https://doi.org/10.1007/bf01718824.
[46] V. Bruss, D. Ganem, Mutational analysis of hepatitis B surface antigen particle assembly and secretion, J. Virol. 65 (7) (1991) 3813–3820.
[47] E.J. Patzer, G.R. Nakamura, C.C. Simonsen, A.D. Levinson, R. Brands, Intracellular assembly and packaging of hepatitis B surface antigen particles occur in the endoplasmic reticulum, J. Virol. 58 (3) (1986) 884–892.
[48] A. Grélard, P. Guichard, P. Bonnafous, S. Marco, O. Lambert, C. Manin, F. Ronzon, E.J. Dufourc, Hepatitis B subvirus particles display both a fluid bilayer membrane and a strong resistance to freeze drying: a study by solid-state NMR, light scattering, and cryo-electron microscopy/tomography, FASEB J. Off. Publ. Fed. Am. Soc. Exp. Biol. 27 (10) (2013) 4316–4326, https://doi.org/10.1096/fj.13-232843.
[49] Y.C. Chen, K. Delbrook, C. Dealwis, L. Mimms, I.K. Mushahwar, W. Mandecki, Discontinuous epitopes of hepatitis B surface antigen derived from a filamentous phage peptide library, Proc. Natl. Acad. Sci. U.S.A. 93 (5) (1996) 1997–2001, https://doi.org/10.1073/pnas.93.5.1997.
[50] W.J. Rutter, P.D.T. Valenzuela, B.D. Hall, G. Ammerer, Synthesis of human virus antigens by yeast, April 8, 2003. US6544757B1.
[51] G. Deléage, C. Combet, C. Blanchet, C. Geourjon, ANTHEPROT: an integrated protein sequence analysis software with client/server capabilities, Comput. Biol. Med. 31 (4) (2001) 259–267, https://doi.org/10.1016/s0010-4825(01)00008-7.
[52] J. Yang, R. Yan, A. Roy, D. Xu, J. Poisson, Y. Zhang, The I-TASSER suite: protein structure and function prediction, Nat. Methods 12 (1) (2015) 7–8, https://doi.org/10.1038/nmeth.3213.
[53] Y. Zhang, J. Skolnick, Scoring function for automated assessment of protein structure template quality, Proteins 57 (4) (2004) 702–710, https://doi.org/10.1002/prot.20264.
[54] D. Kozakov, D.R. Hall, B. Xia, K.A. Porter, D. Padhorny, C. Yueh, D. Beglov, S. Vajda, The ClusPro web server for protein-protein docking, Nat. Protoc. 12 (2) (2017) 255–278, https://doi.org/10.1038/nprot.2016.169.
[55] A. Zlotnick, S.J. Stahl, P.T. Wingfield, J.F. Conway, N. Cheng, A.C. Steven, Shared motifs of the capsid proteins of hepadnaviruses and retroviruses suggest a common evolutionary origin, FEBS Lett. 431 (3) (1998) 301–304, https://doi.org/10.1016/s0014-5793(98)00755-8.
[56] C.A. Orengo, A.M. Martin, G. Hutchinson, S. Jones, D.T. Jones, A.D. Michie, M.B. Swindells, J.M. Thornton, Classifying a protein in the CATH database of domain structures, Acta Crystallogr. D Biol. Crystallogr. 54 (1998) 1155–1167, https://doi.org/10.1107/s0907444998007501. Pt 6 Pt 1.
[57] L.G. Trabuco, E. Villa, K. Mitra, J. Frank, K. Schulten, Flexible fitting of atomic structures into electron microscopy maps using molecular dynamics, Struct. Lond. Engl. 16 (5) (1993) 673–683, https://doi.org/10.1016/j.str.2008.03.005, 2008.
[58] M.A. Lomize, I.D. Pogozheva, H. Joo, H.I. Mosberg, A.L. Lomize, OPM database and PPM web server: resources for positioning of proteins in membranes, Nucleic Acids Res. 40 (2012) D370–D376, https://doi.org/10.1093/nar/gkr703. Database issue.
[59] J.A. Maier, C. Martinez, K. Kasavajhala, L. Wickstrom, K.E. Hauser, C. Simmerling, Ff14SB: improving the accuracy of protein side chain and backbone parameters from Ff99SB, J. Chem. Theor. Comput. 11 (8) (2015) 3696–3713, https://doi.org/10.1021/acs.jctc.5b00255.
[60] C.J. Dickson, B.D. Madej, A.A. Skjevik, R.M. Betz, K. Teigen, I.R. Gould, R.C. Walker, Lipid14: the amber lipid force field, J. Chem. Theor. Comput. 10 (2) (2014) 865–879, https://doi.org/10.1021/ct4010307.